Topological Confinement in Bilayer Graphene

Ivar Martin,[1] Ya. M. Blanter,[2] and A. F. Morpurgo[2]

[1]*Theoretical Division, Los Alamos National Laboratory, Los Alamos, New Mexico, 87544, USA*
[2]*Kavli Institute of Nanoscience, Delft University of Technology, Lorentzweg 1, 2628 CJ Delft, The Netherlands*
(Received 28 September 2007; published 23 January 2008)

We study a new type of one-dimensional chiral states that can be created in bilayer graphene (BLG) by electrostatic lateral confinement. These states appear on the domain walls separating insulating regions experiencing the opposite gating polarity. While the states are similar to conventional solitonic zero modes, their properties are defined by the unusual chiral BLG quasiparticles, from which they derive. The number of zero mode branches is fixed by the topological vacuum charge of the insulating BLG state. We discuss how these chiral states can manifest experimentally and emphasize their relevance for valleytronics.

Most condensed matter systems acquire a gap in single electron excitation spectrum at low temperatures. Typically this happens as a result of spontaneous symmetry breaking, as in the case of superconductors or charge- and spin-density-wave materials. The gap opens due to the interaction of electrons with a slow bosonic mode representing the order parameter (OP). Yet, for certain topologically nontrivial configurations of OP, zero-energy fermionic states reemerge. Examples are Andreev states that form at the domain walls in superconductors [1], states in the superconducting vortex cores [2], and solitons in polyacetylene [3]. Similarly, in cosmology, it has been suggested that our $3 + 1$ dimensional space with its extremely low elementary particle masses may represent a membrane or a string in a higher-dimensional inhomogeneous Higgs vacuum [4]. The *zero modes* may exhibit a number of interesting phenomena, including fermion number fractionalization [5] and chiral anomaly [6]. In condensed matter, similarly to cosmology, the zero modes originate from the Dirac equation, which emerges as an effective (linearized) description of physics near the Fermi surface.

In this Letter we demonstrate that zero modes can also emerge in electrostatically gated bilayer graphene (BLG) structures (Fig. 1). These modes, however, are different from all the examples from condensed matter and high-energy physics that we know of, as they derive not from the Dirac fermions [5,7], but from the unusual low-energy chiral modes of BLG [8,9], which have quadratic dispersion and zero gap between particle and hole bands. When electrostatic bias V is applied between the layers, a gap of the magnitude $|V|$ opens between the particle and hole bands [10]. The interlayer bias plays a role analogous to an OP, but is externally *tunable*. By applying *inhomogeneous* bias one can spatially confine the low-energy states to the regions with low gap, e.g., to a one-dimensional (1D) channel. However, in addition to the conventional confinement by constant-polarity potential, in the case of BLG, there is a possibility of *topological* confinement, with the sign of the confining potential changing across the channel

(Fig. 1). We find that the topological confinement leads to the formation of 1D *chiral* zero modes. In each valley of the graphene band structure there are two such modes (per spin), both carrying electrons in the same direction (opposite for the two valleys). The robustness of the zero modes and their chiral nature are ensured by the topological structure of the gapped bulk states. These modes are likely to influence transport in BLG with smooth potential disorder [11]. They may also have implication for valleytronics [12], as they can enable the fabrication of valley filters and valves, which can be experimentally realized with existing technology.

The low-energy (one-valley) bilayer Hamiltonian with bias $V(x)$ applied between the layers is [8,10]

$$H = \begin{pmatrix} -V(x)/2 & c\pi^\dagger & 0 & 0 \\ c\pi & -V(x)/2 & t_\perp & 0 \\ 0 & t_\perp & V(x)/2 & c\pi^\dagger \\ 0 & 0 & c\pi & V(x)/2 \end{pmatrix}, \quad (1)$$

where c is the Fermi velocity, $\pi = p_x + ip_y$, $\pi^\dagger = p_x - ip_y$, and $t_\perp$ is the interlayer coupling. The Hamiltonian acts in the space of four-component wave functions (ψ_{A1}, ψ_{B1}, ψ_{A2}, ψ_{B2}), where subscript letters represent sublattice and numbers—the layer (we included here only one valley, assuming that $V(x)$ is smooth enough not to cause intervalley transitions). This Hamiltonian provides a good description of BLG as proven by recent experiments [13]. At
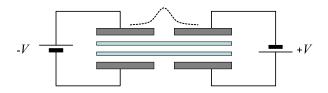

FIG. 1 (color online).   Side view of a gated bilayer graphene configuration with the voltage kink. The region where the interlayer voltage changes sign (channel) supports bands of chiral zero modes (dashed line). The conventional (nontopological) confinement would correspond to the same polarity of bias on both sides of the channel.

low energies and constant gate voltages, $V \ll t_\perp$, the Hamiltonian can be further reduced [14],

$$\tilde{H} = \begin{pmatrix} -\frac{V}{2}\left(1 - \frac{c^2 p^2}{t_\perp^2}\right) & -\frac{c^2 \pi^{\dagger 2}}{t_\perp} \\ -\frac{c^2 \pi^2}{t_\perp} & \frac{V}{2}\left(1 - \frac{c^2 p^2}{t_\perp^2}\right) \end{pmatrix}. \quad (2)$$

Here $p = \sqrt{p_x^2 + p_y^2}$. The remaining components of the wave function have predominantly $A1$ and $B2$ character. The spectrum of the Hamiltonian is

$$E^2 = \frac{V^2}{4}\left(1 - \frac{c^2 p^2}{t_\perp^2}\right)^2 + \frac{c^4 p^4}{t_\perp^2}. \quad (3)$$

At finite bias, the spectrum has a gap which reaches minimum $|V|$ on the circle $cp \approx V/2$. However, as long as $V < t_\perp$, the p^2 correction in the first term can be neglected, simplifying the spectrum to $E^2 = V^2/4 + c^4 p^4/t_\perp^2$. The corresponding term can be also neglected in the diagonal part of $\tilde{H}$. As a result, in the Hamiltonian (2), the V terms and the momentum terms are decoupled. Thus, the transition to the position-dependent potential $V(x)$ corresponds to reinstating the momenta p_x and p_y as differential operators, finally leading to a dimensionless quasiclassical Hamiltonian [15],

$$\mathcal{H}_{qc} = -\varphi(x)\sigma_z - (p_x^2 - p_y^2)\sigma_x - 2p_x p_y \sigma_y$$
$$\equiv \mathbf{g}(\mathbf{p}, x) \cdot \boldsymbol{\sigma}, \quad (4)$$

where we defined $\varphi(x) = V(x)t_\perp a^2/(2c^2)$, and momenta are measured in units of inverse lattice constant a.

For constant $\varphi(x)$ the spectrum has the form $E = \pm\sqrt{\Delta^2 + \epsilon(p)^2}$, which is similar to the spectra of condensed matter systems with off-diagonal long range order; the gate voltage φ plays the role of the order parameter Δ. It is well known that in such systems with a nontrivial topological structure of $\Delta(\mathbf{r})$, low-energy fermionic modes can emerge. Motivated by this analogy, we study related inhomogeneous configurations of $\varphi(x)$.

From Eq. (4), the corresponding wave equation is

$$-\varphi(x)u + (\partial_x + p_y)^2 v = \varepsilon u, \quad (5)$$

$$\varphi(x)v + (\partial_x - p_y)^2 u = \varepsilon v. \quad (6)$$

It possesses a number of symmetries for a general antisymmetric potential profile, $\varphi(-x) = -\varphi(x)$. It is easy to see that in this case for $v(x) = \pm u(-x)$ the two equations (5) and (6) reduce to one. Therefore one can solve two problems separately, for $\Psi = [u(x), u(-x)]$ and $\Phi = [w(x), -w(-x)]$. Furthermore, after we find the eigenvalues and eigenvectors of the first problem for some value of p_y, $\Psi_{p_y}^n = [u_{p_y}^n(x), u_{p_y}^n(-x)]$ and $\varepsilon_{p_y}^n$, the other solution can be obtained as $\Phi_{p_y}^n = [-u_{-p_y}^n(-x), u_{-p_y}^n(x)]$ with eigenvalues $(-\varepsilon_{-p_y}^n)$. Thus in the p_y-ε plane the dispersion of Φ is obtained from the dispersion of Ψ by inversion relative to the point $(0, 0)$. A related, useful symmetry has

to do with the behavior of the spectrum of Eqs. (5) and (6) under $p_y \rightarrow -p_y$. It is easy to see that under this transformation $(u, v) \rightarrow (v, -u)$ and $\varepsilon \rightarrow -\varepsilon$.

Unlike the 1D Dirac equation, which typically describes the domain-wall zero modes [5], Eqs. (5) and (6) are not easily solvable analytically for a general profile $\varphi(x)$. We therefore first analytically study the simple case of step-like potential $\varphi(x) = \varphi_0 \text{sgn}(x)$ and then perform the numerical solution of Eqs. (5) and (6) for a smooth $\varphi(x)$. As we will see, only the details of the zero mode dispersion $\varepsilon(p_y)$ depend on the exact profile of $\varphi(x)$. This is a manifestation of the topological nature of these states.

Step kink.—We first consider a step-like kink, $\varphi(x) = \varphi_0 \text{sgn}(x)$. In this case, both for positive and negative x the potential is constant, and the solution of the wave equation in these regions is $\Psi \propto e^{-\lambda x}$. For the intragap states, i.e., those with $|\varepsilon| < \varphi_0$,

$$\lambda = \pm\alpha \pm i\beta, \quad (7)$$

where $\alpha(\beta) = 2^{-1/2}[(p_y^4 + \varphi_0^2 - \varepsilon^2)^{1/2} + (-)p_y^2]^{1/2}$. For $x < 0$ one should keep only $\lambda_{1,2}^< = -\alpha \pm i\beta$ and for $x > 0$ only $\lambda_{1,2}^> = \alpha \pm i\beta$, with the corresponding wave functions of the form

$$u^{\gtrless}(x) = u_1^{\gtrless} \exp(-\lambda_1^{\gtrless} x) + u_2^{\gtrless} \exp(-\lambda_2^{\gtrless} x). \quad (8)$$

At $x = 0$ the left and right solutions have to be matched. From the structure of the wave equation it is clear that the wave function and its first derivative are continuous across $x = 0$, while the second and higher derivatives are not. Considering for concreteness the states of the form $\Psi = [u(x), u(-x)]$, the matching conditions are

$$u^> = u^<, \quad (9)$$

$$\partial_x u^> = \partial_x u^<, \quad (10)$$

$$\partial_x^2 u^> = \partial_x^2 u^< - 2\varphi_0 u, \quad (11)$$

$$\partial_x^3 u^> = \partial_x^3 u^< + 2p_y(\partial_x^2 u^> - \partial_x^2 u^<) + 2\varphi_0\partial_x u. \quad (12)$$

The third equation is obtained by subtracting Eq. (5) at $x = -0$ from itself at $x = +0$ and using $v(0) = u(0)$. The fourth equation is obtained in the same manner but after first differentiating Eq. (5) over x and using that $\partial_x v(0) = -\partial_x u(0)$. Substituting now the general solutions of Eqs. (8), we obtain a homogeneous system of 4 equations with 4 unknowns which only has a nontrivial solution if its determinant equals zero. Given the form of λ, Eq. (7), this condition is equivalent to

$$4\alpha^2(\alpha^2 + \beta^2) + 4p_y\varphi_0\alpha - \varphi_0^2 = 0. \quad (13)$$

Near zero energy, this equation has a solution only for $p_y < 0$. For $\varphi_0 > 0$, we obtain the dispersion

$$p_y = -(\varepsilon + \varphi_0/\sqrt{2})/(\varepsilon + \varphi_0\sqrt{2})^{1/2} \quad (14)$$

(we analyzed the wave equation near $\varepsilon = 0$ to remove a

spurious branch with $\varepsilon \rightarrow -\varepsilon$). The zero-energy solution is obtained at $p_0 = -\sqrt{\varphi_0}/2^{3/4}$. The other branch corresponding to wave function $\Phi = [-u_{-p_y}(-x), u_{-p_y}(x)]$ has, as discussed above, the inverted dispersion,

$$p_y = (-\varepsilon + \varphi_0/\sqrt{2})/(-\varepsilon + \varphi_0\sqrt{2})^{1/2}. \quad (15)$$

Notice that both solutions have negative velocity near $\varepsilon = 0$. This seems to imply time-reversal symmetry breaking. However, for the second graphene valley, the velocity is positive and thus the symmetry is reinstated. Therefore, the zero modes are chiral; i.e., if we define pseudospin-1/2, with S_y corresponding to the valley index, *all* zero modes have a definite sign of $p_y S_y$. It is also easy to see that on the antikink ($\varphi_0 < 0$) the dispersion is flipped, $\varepsilon(p_y) \rightarrow -\varepsilon(p_y)$.

Note that the decay length of the wave function of the topologically confined states is of the order of $a/\sqrt{\varphi_0} \approx at/\sqrt{Vt_\perp} \gg a$ at low energies. Therefore, our solution is consistent with the long-wavelength expansion (4) used for the description of the system. For kinks wider than $a/\sqrt{\varphi_0}$ one expects *quantitative* deviations, which we indeed find in the direct numerical solution.

Numerical solution.—The wave equations (5) and (6) can be solved for an arbitrary potential profile $\varphi(x)$ numerically using the finite differences method. In Fig. 2 we show an example of an electronic state localized at the kink of the potential $\varphi = \tanh(x/\ell)$ for $\ell = 1$ and $p_y = -1/2^{3/4}$. For the step-like potential this value of p_y would correspond to a zero-energy state. For the rather smooth potential used here, the lowest energy is finite, $\varepsilon = 0.1140$, but indeed much smaller than the reference gap, $\varphi_0 = 1$. The state has the expected symmetry, $v(x) = u(-x)$. The wave function has a slightly oscillatory and decaying behavior, consistent with the complex (nonreal) values of

λ's. A symmetry-related low-energy state $\Phi = (-v, u)$ occurs at $p_y = +1/2^{3/4}$.

In Figs. 3(a)–3(c) we show the intragap state dispersions $\varepsilon(p_y)$ for kinks of various widths. Note that for the narrow kink [panels (a) and (b)] there are only two intragap states, while for the wide kink [panel (c)] more low-energy states appear below the gap edge. In all cases, there are only two (chiral) zero modes per kink per valley per spin regardless of the width. As expected, the analytical result, Eqs. (14) and (15), fits very well for the narrow kink. For comparison, panel (d) shows the dispersion relation for states in a 1D channel defined by "conventional" confinement. In this case no chiral zero modes are present, even though there are states below the gap edge.

Charge of the kink.—It is well known that solitons in 1D systems can carry charge, which can be either rational or irrational [7,16–19]. Similarly, in our case, one might expect that the kink can carry charge. Let us demonstrate that contrary to this expectation the domain-wall charge density is zero. Using the symmetries of the problem, the density in the presence of a kink is proportional to

$$\sum_n \int_{-\infty}^{\infty} |\Psi_{p_y}^n(x)|^2 n_F(\varepsilon_{p_y}^n) = \sum_n \int_0^{\infty} dp_y |\Psi_{p_y}^n(x)|^2.$$

Due to the completeness of the eigenfunctions, this expression is an x-independent constant proportional to the momentum (energy) cutoff.

Topological considerations.— Above we found that in the presence of a kink there are two zero modes per graphene valley per spin. We now demonstrate how the appearance of these modes can be understood from topological considerations [20]. The number of zero modes, or more precisely the number of zero-energy left movers minus the number of zero-energy right movers is related to the topological charge N_3 of the Fermi point located in the extended quasiclassical 3D momentum-real space
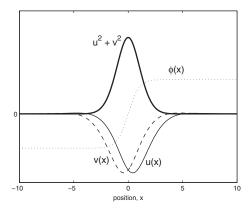

FIG. 2. Spatial structure of the confined state obtained numerically from Eqs. (5) and (6) for particular value $p_y = -1/2^{3/4}$. The energy of the state is $\varepsilon = 0.1140$. Shown are the components u and v of the wave function (thin and dashed lines, respectively), the probability density $|\Psi|^2 = u^2 + v^2$ (thick line), and the potential profile, taken here as $\varphi(x) = \tanh(x)$. Note the symmetry, $u(x) = v(-x)$.
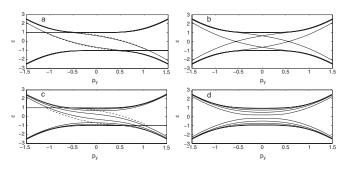

FIG. 3. Energy level structure in the presence of nonuniform interlayer bias $\varphi(x)$. The low-energy states in (a) and (c) are localized on the single kink of profile $\varphi(x) = \tanh(x/\ell)$ with $\ell = 0.5$ and $\ell = 4$, respectively. For (a) and (c) we used open boundary conditions, $\Psi(\pm20) = 0$, which caused flat bands at $\varepsilon = \pm1$. The dashed lines are the analytical expressions for the intragap state dispersion, Eq. (14). (b) Same as (a) but with kink and antikink at $x = \pm10$ and periodic boundary conditions. (d) Nontopological confinement for potential profile $\varphi(x) = \tanh^2(x/4)$. Note the absence of chiral zero modes.

$(\mathbf{p}, x)$. In terms of the quasiclassical Green function, $\mathcal{G}_{qc} = (ip_0 - \mathcal{H}_{qc})^{-1}$,

$$N_3 = \frac{1}{24\pi^2} e_{ijkl} \mathrm{tr} \int_{\sigma_3} dS^l \mathcal{G}_{qc} \partial_i \mathcal{G}_{qc}^{-1} \mathcal{G}_{qc} \partial_j \mathcal{G}_{qc}^{-1} \mathcal{G}_{qc} \partial_k \mathcal{G}_{qc}^{-1},$$

where integration is to be performed over an arbitrary 3D surface σ_3 enclosing the Fermi point $(p_0, \mathbf{p}, x) = (0, \mathbf{0}, 0)$. The charge N_3 is the degree of the mapping of σ_3 onto a manifold corresponding to the $\mathcal{G}_{qc}$. Given the form of $\mathcal{H}_{qc}$, this manifold is equivalent to a 3D sphere, and thus the mapping belongs to the nontrivial $\pi_3(S^3)$ homotopy group. In evaluating N_3, two choices of σ_3 are particularly useful: (a) infinite planes $p_y = \pm p_y^0$ and (b) infinite planes at $x = \pm x^0$ (assuming that the planes are sufficiently close, the flux contributing to N_3 but not crossing these planes is negligible). Representation (a) is equivalent to the quasiclassical expansion of the difference of spectral asymmetry functions, $\nu = \nu(p_y^0) - \nu(-p_y^0)$, where

$$\nu(p_y) = \mathrm{tr} \int \frac{dp_0}{2\pi i} \mathcal{G} \partial_{p_0} \mathcal{G}^{-1} = -\frac{1}{2} \sum_n \mathrm{sgn}\, \varepsilon_{p_y}^n.$$

ν counts the number of dispersion branches that cross zero energy from above on the interval $[-p_y^0, p_y^0]$. In representation (b), N_3 is nothing but the difference of the vacuum topological charges of the insulating states to the right and to the left of the domain wall, $\tilde{N}_3(x^0) - \tilde{N}_3(-x^0)$. Given the form of $\mathcal{H}_{qc}$, Eq. (4),

$$\tilde{N}_3(x_0) = \frac{1}{4\pi} \int dp_x dp_y \frac{1}{|\mathbf{g}|^3} \mathbf{g} \cdot [\partial_{p_x} \mathbf{g} \times \partial_{p_y} \mathbf{g}],$$

from which one easily finds $\tilde{N}_3(x_0) = \mathrm{sgn}[\varphi(x^0)]$. Thus, for $\varphi(+\infty) > 0$, we obtain $N_3 = \tilde{N}_3(x_0) - \tilde{N}_3(-x_0) = \nu = 2$, consistent with our earlier finding that there are two branches per kink per valley per spin that cross zero energy with negative velocity.

Having established the presence of one-dimensional chiral zero modes originating from topological confinement, we briefly discuss their relevance to one area of current interest, namely, "valleytronics," which attempts to utilize the valley degree of freedom to achieve new electronic functionality [12]. As we have shown above [e.g., see Figs. 3(a) and 3(c)], a topologically confined 1D channel contains zero modes, with the direction of propagation determined by the valley. Thus, a *valley filter* is realized when a voltage difference is applied along the kink—only electrons in one of the valleys will carry the current and the other valley is "filtered out." It should be possible to realize a *valley valve* by "connecting" two filters in series. When the polarity of two filters is the same, the current can pass through; for opposite polarities the current is blocked. We note that earlier proposals [12,21] for valley filters and valves in graphene monolayers relied on perfect zigzag edges, making their practical realization very challenging. On the other hand, the technology needed for valley filter and valve using the topologically confined channels is much less demanding: A smooth 1D channel can easily be realized away from the edges of the graphene sample, thus decreasing substantially the possibility of intervalley scattering. Some of the technology—the opening of a gap in a bilayer using gate electrodes—has already been demonstrated experimentally [22]. A more detailed discussion of valley filtering induced by topological confinement will be presented elsewhere [23].

[1] I. O. Kulik, Zh. Eksp. Teor. Fiz. **57**, 1745 (1969) [Sov. Phys. JETP **30**, 944 (1970)].
[2] C. Caroli, P. G. de Gennes, and J. Matricon, Phys. Lett. **9**, 307 (1964).
[3] W. P. Su, J. R. Schrieffer, and A. J. Heeger, Phys. Rev. Lett. **42**, 1698 (1979).
[4] V. A. Rubakov and M. E. Shaposhnikov, Phys. Lett. **125B**, 136 (1983).
[5] R. Jackiw and C. Rebbi, Phys. Rev. D **13**, 3398 (1976).
[6] V. Rubakov, *Classical Theory of Gauge Fields* (Princeton University, Princeton, NJ, 2002).
[7] C.-Y. Hou, C. Chamon, and C. Mudry, Phys. Rev. Lett. **98**, 186809 (2007).
[8] E. McCann and V. I. Fal'ko, Phys. Rev. Lett. **96**, 086805 (2006).
[9] G. E. Volovik, in *Quantum Analogues: From Phase Transitions to Black Holes and Cosmology*, Springer Lecture Notes in Physics Vol. 718, edited by W. G. Unruh and R. Schützhold (Springer-Verlag, New York, 2007), pp. 31–73.
[10] E. McCann, Phys. Rev. B **74**, 161403 (2006).
[11] J. Martin *et al.*, arXiv:0705.2180.
[12] A. Rycerz, J. Tworzydlo, and C. W. J. Beenakker, Nature Phys. **3**, 172 (2007).
[13] K. S. Novoselov *et al.*, Nature Phys. **2**, 177 (2006); T. Ohta *et al.*, Science **313**, 951 (2006).
[14] J. L. Mañes, F. Guinea, and M. A. H. Vozmediano, Phys. Rev. B **75**, 155424 (2007).
[15] We have verified by a direct numerical calculation that such a reduced Hamiltonian well approximates the full Hamiltonian (1).
[16] J. Goldstone and F. Wilczek, Phys. Rev. Lett. **47**, 986 (1981).
[17] M. J. Rice and E. J. Mele, Phys. Rev. Lett. **49**, 1455 (1982).
[18] R. Jackiw and G. Semenoff, Phys. Rev. Lett. **50**, 439 (1983).
[19] S. Kivelson, Phys. Rev. B **28**, 2653 (1983).
[20] G. E. Volovik, *The Universe in a Helium Droplet* (Clarendon, Oxford, 2003), Chap. 22.
[21] P. Recher *et al.*, Phys. Rev. B **76**, 235404 (2007).
[22] J. B. Oostinga *et al.*, Nat. Mater. AOP doi:10.1038/nmat/ 2082 (2007).
[23] I. Martin, Ya. M. Blanter, and A. F. Morpurgo (to be published).